

Optimization of the operating conditions in inductively coupled plasma optical emission spectrometry

N.S. Velitchkova^{1*}, S.V. Velichkov², M. G. Karadjov¹, N. N. Daskalova²

¹Geological Institute, Bulgarian Academy of Sciences,
Acad. G. Bontchev Str., bl. 24, 1113 Sofia, Bulgaria

²Institute of General and Inorganic Chemistry, Bulgarian Academy of Sciences,
Acad. G. Bontchev Str., bl. 11, 1113 Sofia, Bulgaria

Received November 8, 2016; Revised December 22, 2016

Optimization of the plasma operating conditions was carried out in aspect to achieve the lowest possible detection limits by using radial viewing 40.68 MHz inductively coupled plasma optical emission spectrometry (ICP-OES). Mg II 280.270 nm / Mg I 285.213 nm line intensity ratios (Mg II / Mg I) was measured to evaluate the robustness of the plasma operating conditions. The operating conditions were affected by varying: incident power, carrier and sheathing gas flow rates. The relationship between the magnitude of Mg II / Mg I ratios and excitation temperature in ICP was obtained. The results show that the excitation conditions in ICP have to be modified only by varying the incident power and the sheathing gas flow rates at an optimal value of the carrier gas flow rate. In this case the aerosol formation and transport processes are the same under different excitation conditions in ICP. The excitation conditions from non robust to robust were varied for minimization of the detection limits in the determination of elements by using the selected prominent lines with different spectral characteristics in the presence of “pure” and complex matrices.

Keywords: ICP-OES, Optimization of operating condition, Traces of elements, Detection limits

INTRODUCTION

The optimization of the operating conditions was carried out in aspect to lower the detection limits by radial viewing inductively coupled plasma optical emission spectrometry (ICP-OES). The optimization procedure includes the following steps: line selection according to the absence or the lowest possible level of spectral interference; influence of the operating parameters (incident power, carrier and sheathing gas flow rates) on the net line and background intensities [1].

The sensitivities of different line intensity ratios were used to control the excitation conditions in ICP-OES. The Mg II 280.270 nm/Mg I 285.213 nm line intensity ratios (Mg II/Mg I) was found to remain a good compromise to follow the change in the plasma conditions. An advantage of this ratio is to be independent of the detector. Therefore, the absolute value of the ratio Mg II / Mg I can be used also for comparison of different ICP systems and operating conditions. This ratio has been widely used and is an appropriate test [2].

Some authors pay attention on the calculation of correction factor for the magnesium atom to ion line intensity signals when a blank solution is contaminated by magnesium [3]. There should be noted, that depending on the optical system, the two

magnesium lines may be located in adjacent orders, or at different locations within the same order, it may be necessary to compensate for a different wavelength response. A simple way to establish a correction factor is to assume that the continuum has a constant value in the range from 280 to 285 nm. It is then sufficient to measure the background emission at 280.2 nm and 285.2 nm [2]. Therefore, the background must be measured in the spectral windows around the corresponding magnesium spectral lines. In addition, when a blank solution is contaminated by magnesium, the background signals should be measured in λ_a of corresponding magnesium lines in order to obtain correct net line signals for the both magnesium lines.

Analytical performance in the optimization of an ICP-OES in order to minimize both the spectral interference level and the detection limits in the presence of line rich emission matrices requires the optimum line selection. The optimum line selection for trace analysis requires the choice of prominent lines free or negligibly influenced by line interference. This is the first essential optimization step [4, 5].

A large number of research groups have investigated the non-spectral matrix effects in order to suppress or eliminate this type of interference. The robust plasma conditions are more appropriate when compared to the non-robust plasma conditions. The

* To whom all correspondence should be sent.
E-mail: niaveli@geology.bas.bg

general conclusion from the investigations was that the total elimination of error from non-spectral interferences cannot be achieved under robust operating conditions, but only by precise matching of the acid and matrix contents in both the reference and the sample solutions [6-9].

Studies on the impact of operating conditions on the detection limits require the signal - to background ratios to be maximized and the relative standard deviation of the background signal to be minimized [1, 10, 11].

The purpose of the present paper is to investigate the possibilities of radial viewing 40.68 MHz ICP-OES to achieve the lowest possible detection limits by optimizing of the operating conditions. For this purpose the following data have been compiled by varying the carrier gas flow rate, incident power and sheathing gas flow rate:

(i) Different Mg II /Mg I line intensity ratios for control of the robustness of the plasma excitation conditions;

(ii) Relationship of the Mg II / Mg I and the excitation temperature (T_{exc});

(iii) Application of the methodology for optimization of the operating conditions in order to obtain the lowest possible detection limits in pure solvent and the true detection limits in the presence of "pure" and complex matrices.

EXPERIMENTAL

Instrumentation

The experiments were performed with a radial viewing ICP-OES system ULTIMA 2, Horiba group, Jobin Yvon, (Longjumeau, France), Meinhard nebulizer type P/N ER 2050 – 0710N and high dynamic detector based on photomultiplier tubes. The operating conditions were affected by different constant and variable parameters.

Reagents and test solutions

The concentration of magnesium in test solution for the plasma robustness measurement was $10 \mu\text{g ml}^{-1}$ and the concentration of titanium in solution for the temperature measurement was $8 \mu\text{g ml}^{-1}$.

In the determination of Sc, Y, La, Ce, Nd, Sm, Eu, Gd, Tb, Dy, Ho, Er, Tm and Yb the pure solvent contains 22 mg ml^{-1} solution of hydrochloric acid in double – distilled water. In the determination of rare earth elements (REE's) in lutetium oxide, the solutions contain all analytes and 8.79 mg ml^{-1} lutetium.

In the determination of Ce, Nd, Eu, Yb, Tm, Ga, Cr, Nb, Ni, Mn, Ge and Zr as dopants in single

crystals of potassium titanylphosphate (KTP) the pure solvent contains $142 \text{ mg ml}^{-1} \text{ H}_2\text{SO}_4$ and approximately $0.02 \text{ mg ml}^{-1} \text{ H}_2\text{O}_2$. The final concentration of KTP matrix was 8 mg ml^{-1} , $142 \text{ mg ml}^{-1} \text{ H}_2\text{SO}_4$ and approximately $0.02 \text{ mg ml}^{-1} \text{ H}_2\text{O}_2$. Plastic or polytetrafluoroethylene ware was used throughout.

RESULTS AND DISCUSSION

Evaluation of the robustness of the operating conditions by Mg II / Mg I in ICP

The operating conditions were affected by varying:

(i) Carrier gas flow rate and sheathing gas flow rate at a constant value of incident power;

(ii) Incident power and the sheathing gas flow rate, whereas the carrier gas flow rate remained a constant value (0.4 l min^{-1}). This is an optimal value for carrier gas flow rate, in accordance with the recommendations for the Meinhard nebulizer.

Influence of carrier gas flow rate and sheathing gas flow rate at a constant value of the incident power

The effect of carrier and sheathing gas flow rates as variable parameters at a constant value of incident power of 1000 W on the Mg II / Mg I in pure solvent is presented in Figure 1.

Three different shape curves were obtained:

(i) The bell-shaped curves were derived by varying:

- By varying the carrier gas flow rates from 0.2 l min^{-1} to 0.7 l min^{-1} (without sheath gas flow) (Fig. 1, curve 1). The highest of Mg II / Mg I ratios were obtained at carrier gas flow rates from 0.4 to 0.6 l min^{-1} i.e., at optimal carrier gas flow rates for this type of nebulizer, which ensures the highest efficiency. This value is noted from the manufacturer for each type of nebulizer separately;

- By varying sheath gas flow rates from 0 to 1.0 l min^{-1} at a constant value of the carrier gas flow rates 0.2 l min^{-1} (Fig. 1 curve 2). The carrier gas flow rate of 0.2 l min^{-1} (without sheath gas) is lower than the optimal rate. This value is not enough for an effective transfer of the aerosols to the inductively coupled plasma. The net line signals of Mg II 280.270 nm and Mg I 285.213 nm as well as the corresponding Mg II / Mg I ratios are very low. By adding 0.2 l min^{-1} sheath gas, the Mg II / Mg I ratios increase significantly, because here the sheath gas flow rate ensures more effective transport of the aerosols to the plasma and more effective exchange of the energy between the high frequency field and the central channel.

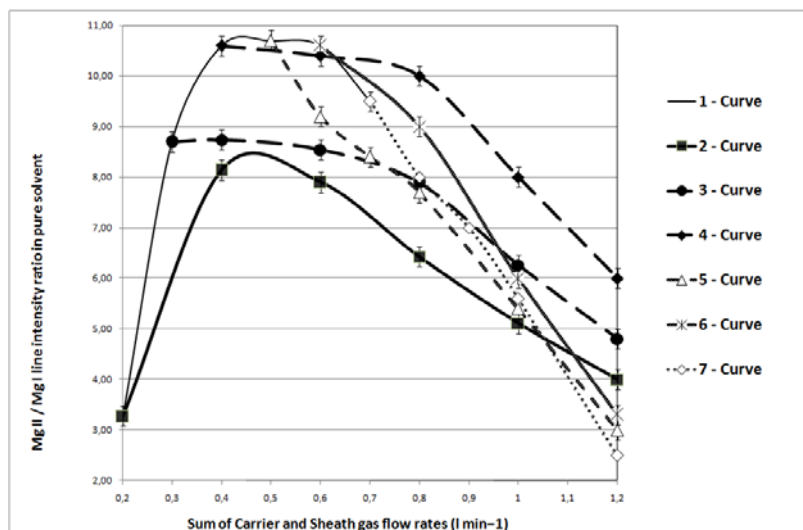


Fig. 1. Effect of carrier and sheathing gas flow rates as variable parameters at a constant value of incident power (1 000 W) on the Mg II / Mg I in pure solvent: **Curve 1** - variable carrier gas flow rates without sheathing gas; **Curve 2** - constant carrier gas flow = 0.2 l min⁻¹ + variable sheathing gas; **Curve 3** - constant carrier gas flow = 0.3 l min⁻¹ + variable sheathing gas; **Curve 4** - constant carrier gas flow = 0.4 l min⁻¹ + variable sheathing gas; **Curve 5** - constant carrier gas flow = 0.5 l min⁻¹ + variable sheathing gas; **Curve 6** - constant carrier gas flow = 0.6 l min⁻¹ + variable sheathing gas and **Curve 7** - constant carrier gas flow = 0.7 l min⁻¹ + variable sheathing gas.

The exchange of energy between the high frequency field and the central channel is critical [12].

Therefore, the bell-shaped curves can be obtained when the investigation of the relation between Mg II / Mg I ratios and the carrier gas flow rates begins with a value of carrier gas lower than the corresponding optimal value for a given nebulizer.

(ii) The second types of curves are with plateau (Fig. 1, curves 3 and 4). The constant value of the magnitude of the Mg II / Mg I ratios were derived in both cases:

- Carrier gas flow rate 0.3 l min⁻¹ and sum of carrier and sheath gas flow rates 0.4 l min⁻¹ + 0.2 l min⁻¹ (Fig. 1, curves 3);

- Carrier gas flow rate 0.4 l min⁻¹ and sum of carrier and sheath gas flow rates 0.4 l min⁻¹ + 0.2 l min⁻¹ (Fig. 1 curves 4).

The influence of energy transfer between the plasma and the injected species was found to be insignificant by adding 0.1 or 0.2 l min⁻¹ sheath gas flows to the 0.3 or 0.4 l min⁻¹ to the carrier gas flow [12]. Here the Mg II / Mg I ratio remains constant. Further, by increasing of the sheath gas at the above mentioned constant carrier gas flow rates, the Mg II / Mg I ratio decrease slightly (Table 1, Fig. 1, curves 3 and 4).

(iii) The third type of curves show, that with the increase of the sheath gas flow rates at constant carrier gas flow rates 0.5, 0.6 or 0.7 l min⁻¹, the magnitude of the Mg II / Mg I ratio decrease (Fig. 1, curves 5, 6 and 7). Under these experimental

conditions the sheath gas flow rates influence significantly the energy transfer between the plasma and the injected species and the magnitude of the Mg II / Mg I ratio decrease. The laminar sheath gas and the carrier gas enter into the plasma separately (without mixing) and influence in a different way the processes in the inductively coupled plasma [12].

There should be underlined that in the literature different curve shapes are published for inductively coupled plasmas (radial and axial viewing), by using different type of nebulizers and spray chambers [13 - 21]. In the present paper all types of curves were obtained by using a radial viewing 40.68 MHz ICP and Meinhard nebulizer, type P/N ER 2050 – 0710N. The relative standard deviation in the determination of the Mg II/Mg I ratios is 5%.

Influence of incident power and sheathing gas flow rate on the Mg II / Mg I ratio in pure solvent at a constant value of carrier gas flow rate

The corresponding results for different values of incident power and sum of carrier and sheathing gas flow rates are shown on the Fig. 2, A and B. The following conclusions can be drawn:

(i) The magnitude of the Mg II / Mg I ratios do not change for a sum of carrier and sheathing gas flow rates between 0.4 and 0.6 l min⁻¹ for different values of incident power in pure solvent (Fig. 2 A and B). Probably for a sheathing gas flow rate of 0.2 l min⁻¹, the energy transfer between the plasma and the injected species is not influenced [12], regardless of the magnitude of incident power. Further, with increasing of the sheathing gas flow rate, the Mg II /

Mg I decreases. The shape of the curves (Fig. 2A) follow the same pattern as the curves 3 and 4 (Fig. 1). By increasing the sum of carrier and sheathing gas flow rates higher than 0.6 l min⁻¹ the Mg II / Mg I ratios decrease and follow the shape of the curves, shown on Fig.1 (curves 5, 6 and 7).

(ii) Higher Mg II / Mg I ratios are obtained with a lower sum of carrier and sheathing gas flow rates for a given incident power. The Mg II / Mg I ratios increase with the increasing of the incident power for all sums of carrier and sheathing gas flow rates (Fig.2, A).

(iii) Equal Mg II/Mg I ratios can be obtained for different combinations of sums of carrier and sheathing gas flow rates and incident powers.

Relationship between the Mg II / Mg I ratio and the plasma excitation temperature (T_{exc})

The relationship between the magnitude of Mg II /Mg I and T_{exc} in a pure solvent was derived. The T_{exc} was measured by the Boltzmann plot method with titanium lines for nine combinations between incident power and sheathing gas flow rates [22].

Five values for the T_{exc} were obtained with each of the eight combinations (Table 1, column 3). In all

cases T_{exc} ± 200 K was obtained. The results show that higher Mg II / Mg I ratios correspond to higher values of T_{exc}.

It could be concluded that the excitation conditions in ICP have to be modified by varying the incident power and the sheathing gas flow rates at an optimal value for the carrier gas flow rate, in accordance with the recommendations for the Meinhard nebulizer. The equipment with sheathing gas device gives possibility to change the ionization and excitation conditions of the plasma by varying the sheathing gas flow and the incident power at a constant optimal value of the carrier gas. The carrier flow is not only a very critical parameter of the ICP but also a nebulizer parameter that governs the amount of aerosol carried to the plasma [1]. At constant optimal value of carrier gas flow rate the aerosol formation and transport processes do not change under different excitation conditions in ICP.

There should be noted that by using ICP-OES equipments without sheathing gas device, the change of the operating conditions can be achieved by varying the incident power at an optimal carrier gas flow rate.

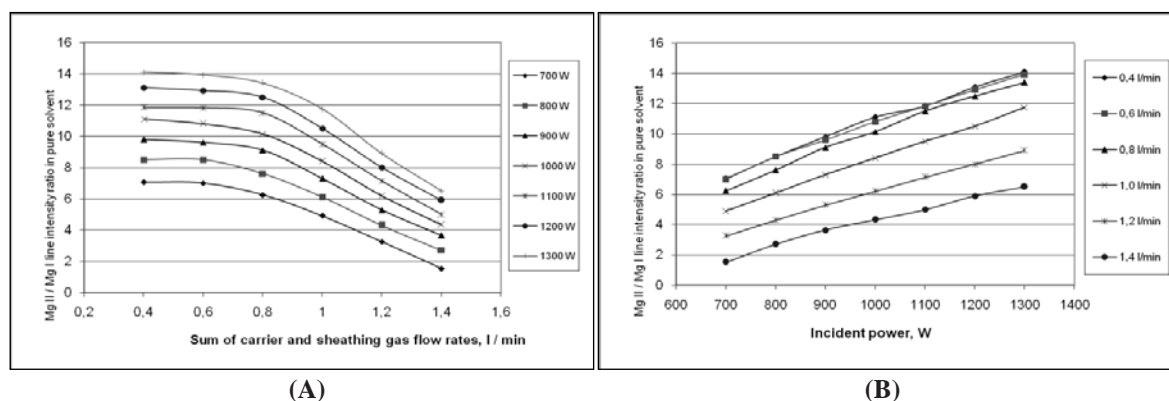


Fig.2. Effect of incident power (A) and sheathing gas flow rate (B) on the Mg II / Mg I ratio in pure solvent at a constant value of carrier gas flow rate

Table 1. Type of operating conditions obtained at a constant optimal value of the carrier gas flow rate of 0.4 l min⁻¹, variable sheathing gas flow rate and incident power

Type of operating conditions	Mg II / Mg I	T _{exc} , K	Incident power, W	Sum of carrier and sheathing gas flow rates, l min ⁻¹
Non-robust	1.8	5200 ± 200	700	1.4 = 0.4 + 1.0
	3.6	6000 ± 200	700	1.2 = 0.4 + 0.8
Semi-robust	6.0	6580 ± 200	800	1.0 = 0.4 + 0.6
	6.0	6580 ± 200	1 000	1.2 = 0.4 + 0.8;
Robust	11	7200 ± 200	1 000	0.4 = 0.4 + 0
	11	7200 ± 200	1 100	0.8 = 0.4 + 0.4
	12	7500 ± 200	1 100	0.6 = 0.4 + 0.2
	12	7500 ± 200	1 200	0.8 = 0.4 + 0.4

Table 1 summarizes the type of excitation conditions, which were obtained by radial viewing

40.68 MHz ICP. Hence, by varying the excitation conditions from non-robust to robust (Table 1) the

lowest possible detection limits in pure solvent and in the presence of different matrices can be achieved. The above mentioned methodology was applied for optimization of the operating conditions in order to minimize the detection limits in the determination of trace of elements in the presence of different matrix constituents.

Minimization of the true detection limits in the determination of Sc, Y, La, Ce, Pr, Nd, Sm, Eu, Gd, Tb, Dy, Ho, Er, Tm and Yb in pure solvent and in the presence of 10 mg ml⁻¹ lutetium oxide (8.79 mg ml⁻¹ lutetium) as matrix

Lutetium is a typical rare earth element characterized by a full f-level. This element emits a relatively smaller number of spectral lines in comparison to the REEs from cerium to erbium. Besides, in the presence of matrix lutetium, the strong LuO bands have been registered at $T_{exc} \approx 6200$ K around the prominent lines of La, Ce, Pr, Nd, Sm and Eu. The intensities of the molecular bands considerably decrease or disappear altogether at $T_{exc} \approx 7200$ K. Optimal line selection for trace analysis require the choice of the prominent lines free or negligibly influenced by line interference [4].

The detection limits in pure solvent were calculated in accordance to Eq. (1) [1]:

$$C_L = 2\sqrt{2} \times 0.01 \times RSDB \times BEC \quad (1)$$

The true detection limit ($C_{L\ true}$) in the presence of "pure" rare earth matrices was expressed by Q - values for line interference [$Q_I(\lambda_a)$] and wing background interference [$Q_W(\Delta\lambda_a)$] levels, respectively in accordance with (Eq. (2)) [4].

$$C_{L\ true} = 2/5 Q_I(\lambda_a) \times C_1 + 2\sqrt{2} \times 0.01 \times RSDBL \times [BEC + Q_I(\lambda_a) \times C_1 + Q_W(\Delta\lambda_a) \times C_1] \quad (2)$$

The magnitude of [$Q_I(\lambda_a)$] values is of primary importance for the magnitude of the true detection limits. The influence of the wing background interference levels [$Q_W(\Delta\lambda_a)$] is negligible (Eq. 2).

The effect of the operating conditions (varying from non-robust to robust) on the magnitude of background equivalent concentration in pure solvent (BEC), [$Q_I(\lambda_a)$] values for line interferences and

[$Q_W(\Delta\lambda_a)$] values for wing interferences in the presence of 8.79 mg ml⁻¹ lutetium for the selected analysis lines of Sc, Y, La, Ce, Pr, Nd, Sm, Eu, Gd, Tb, Dy, Ho, Er, Tm and Yb were studied. The lowest values of BEC, [$Q_I(\lambda_a)$] and [$Q_W(\Delta\lambda_a)$] values were measured at Mg II / Mg I ratio of about 3.6 which corresponds to ($T_{exc} \approx 6000$ K).

By using BEC, [$Q_I(\lambda_a)$] and [$Q_W(\Delta\lambda_a)$] values in the presence of 8.79 mg ml⁻¹ lutetium as matrix, which were measured under different excitation conditions (non-robust, semi robust and robust) (Table 1), the detection limits in pure solvent by (Eq. 1) and the true detection limits by Eq.(2) were obtained.

Figure 3 A and B shows the relationships between the Mg II / Mg I ratios and the detection limits in pure solvent (A) and the true detection limits in the presence of 8.79 mg ml⁻¹ lutetium in solution (B).

In conclusion, the non-robust conditions at $T_{exc} \approx 6000$ K (Mg II / Mg I = 3.6) proved to be more appropriate for the determination of traces of REE's in a pure solvent and in the presence of 8.79 mg ml⁻¹ lutetium as a matrix as compared to the robust conditions. The detection limits under non-robust excitation conditions at $T_{exc} \approx 6000$ K (Mg II / Mg I = 3.6) are between 3 and 6 times lower than under robust excitation conditions at $T_{exc} \approx 7200$ K (Mg II / Mg I = 10) in pure solvent as well as in the presence of lutetium oxide as a matrix for the analytes Sc, Y, La, Pr, Sm, Eu, Gd, Tb, Dy, Ho, Er, Tm and Yb.

Q-values due to LuO molecular bands for the analysis lines of cerium (Ce II 413.765 nm) and neodymium (Nd II 401.225 nm) decrease with the increase of the Mg II / Mg I ratio in the presence of a lutetium matrix. Q-values for line interference [$Q_I(\lambda_a)$] are equal to zero for Mg II / Mg I from 9 or 11 in the case of Nd II 401.225 nm or Ce II 413.380 nm, respectively, i.e. at an $T_{exc} \approx 7200$ K [4]. In addition the sums of the ionization and excitation potentials for the ionic prominent lines of REE's vary from 8.9 to 10.0 V [23, 24]. This conclusion is in accordance with [25].

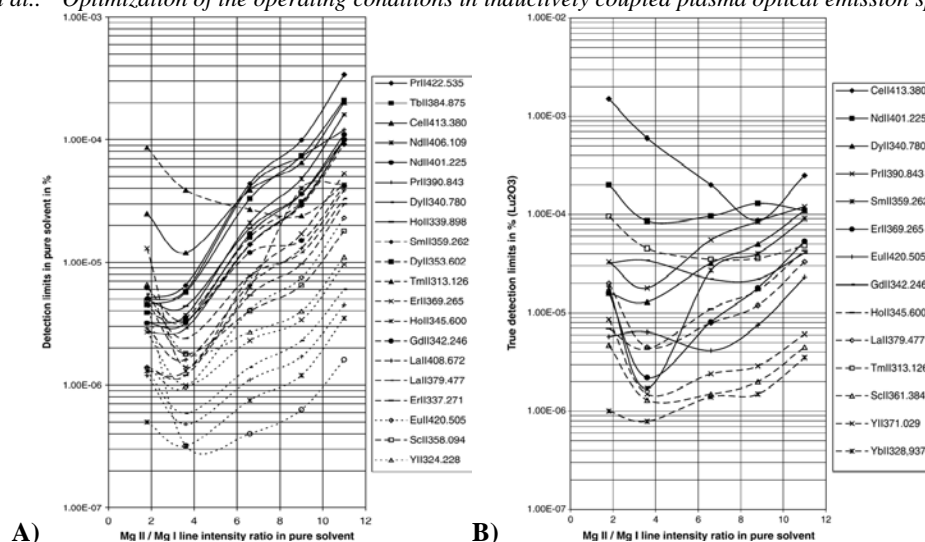


Fig. 3. Relationship between Mg II 280.270 nm / Mg I 285.213 nm line intensity ratios and the detection limits in pure solvent (A) and the true detection limits in the presence of 8.79 mg ml⁻¹ lutetium in solution (B)

By using the selected prominent lines (in nm) the following detection limits (in %) were reached:

(i) Detection limits in pure solvent (C_L) (in %): Sc II 358.094 - 1.9×10^{-6} , Y II 324.228 - 1.8×10^{-6} , Y II 360.073 - 1.0×10^{-6} , Y II 360.073 - 1.0×10^{-6} , La II 408.672 - 1.0×10^{-6} , Ce II 413.380 - 1.1×10^{-5} , Pr II 422.293 - 6.5×10^{-6} , Nd II 406.109 - 3.3×10^{-6} , Sm II 359.260 - 4.3×10^{-6} , Eu II 420.505 - 1.0×10^{-6} , Gd II 342.247 - 3.4×10^{-6} , Tb II 356.852 - 5.7×10^{-6} , Dy II 353.602 - 4.0×10^{-6} , Ho II 339.898 - 4.4×10^{-6} , Er II 337.271 - 1.3×10^{-6} , Tm II 313.126 - 3.9×10^{-5} , Yb II 328.937 - 3.0×10^{-7} and Lu II 261.542 - 3.0×10^{-7} .

(ii) True detection limits ($C_{L \text{ true}}$) in the presence of 8.79 mg ml⁻¹ lutetium as matrix (in %): Sc II 361.384 - 1.3×10^{-6} , Y II 371.030 - 1.5×10^{-6} , La II 379.478 - 4.5×10^{-6} , Ce II 413.765 - 8.7×10^{-5} , Pr II 390.844 - 1.8×10^{-5} , Nd II 401.225 - 1.1×10^{-4} , Sm II 359.260 - 1.2×10^{-5} , Eu II 420.505 - 6.4×10^{-6} , Gd II 342.247 - 3.4×10^{-5} , Tb II 384.873 - 1.4×10^{-5} , Dy II 340.780 - 1.3×10^{-5} , Ho II 345.600 - 4.3×10^{-6} , Er II 369.265 - 2.2×10^{-6} , Tm II 313.126 - 4.5×10^{-5} , Yb II 328.937 - 7.9×10^{-7} .

There would be noted that in the case of a lutetium matrix, for Ce and Nd the lowest detection limits were obtained under robust excitation conditions. The LuO bands registered around Ce II 413.380 nm and Nd II 401.225 nm disappeared at higher excitation temperatures [4]. In the presence of a lutetium matrix, the line interference level is lower in comparison with the rare earth matrices from cerium to erbium and the worsening of the true detection limit is negligible in comparison with the detection limits in pure solvent.

Minimization of the true detection limits in presence of 8 mg ml⁻¹ KTP

Single crystals of potassium titanylphosphate (KTP) doped with Ce, Nd, Eu, Yb, Tm, Ga, Cr, Nb, Ni, Mn, Ge and Zr are excellent materials for electrooptical applications and laser technique. The methodology for optimization was applied by using the selected analysis lines [5]. Tables 2 and 3 present the selected prominent lines (columns 1) with different sums of ionization and excitation potentials (columns 2) and true detection limits (in %) with respect to the dissolved solid (8 mg ml⁻¹ KTP in solution) (columns 3).

The results from Tables 2 and 3 demonstrate that by varying T_{exc} , the plasma emits spectral lines with different net line signals depending on the sums of the ionization and excitation potentials of the selected ionic analysis lines.

Table 2. True detection limits ($C_{L \text{ true}}$) for Ce, Nd, Eu, Yb, Tm and Ga with respect to the dissolved solid in solution for solid concentration of 8 mg ml⁻¹ KTP (in %)

Selected analysis lines, λ , nm	Optimal excitation temperature $T_{\text{exc}} \approx 6000$ K (Mg II / Mg I = 3.6)	
	Sum = ionization + excitation potentials, (V) [23, 24]	$C_{L \text{ true}}$ (%)
Ce II 413.380	9.33	2.6×10^{-4}
Nd II 406.109	9.01	6.6×10^{-4}
Eu II 381.967	8.91	1.0×10^{-5}
Yb II 328.937	10.02	3.3×10^{-5}
Tm II 317.283	10.02	4.0×10^{-5}
Ga I 294.364	10.31	1.3×10^{-4}

Table 3. True detection limits ($C_{L \text{ true}}$) for Nb, Ni, Mn, Ge and Zr with respect to the dissolved solid in solution for solid concentration of 8 mg ml⁻¹ KTP (in %)

Optimal excitation temperature $T_{\text{exc}} \approx 7200$ K (Mg II / Mg I = 10)		
Selected analysis lines, λ , nm	Sum = ionization + excitation potentials, (V) [23, 24]	$C_{L \text{ true}}$ (%)
Nb II 269.706	11.63	2.0×10^{-4}
Ni II 221.647	14.26	1.6×10^{-4}
Mn II 257.610	12.14	2.5×10^{-5}
Ge II 265.158	12.57	1.6×10^{-2}
Zr II 343.823	12.53	4.6×10^{-5}

The lowest true detection limits for the elements Ce, Nd, Eu, Yb, Tm, Ga were obtained at optimal excitation temperature $T_{\text{exc}} \approx 6000$ K (Mg II / Mg I = 3.6). The sum of the ionization and excitation potentials for the ionic prominent lines of rare earth elements varies from 8.9 V to 10.3V (Table 2, column 2) [23, 24]. For Cr, Nb, Ni, Mn, Ge and Zr the lowest true detection limit were obtained at optimal excitation temperature $T_{\text{exc}} \approx 7200$ K (Mg II / Mg I = 10) in pure solvent and in the presence of a KTP matrix. The sum of the ionization and excitation potentials for the ionic prominent lines of these elements varies from 11.6 V to 14.26 V (Table 3, column 2) [23, 24].

CONCLUSIONS

Improvement of the detection limits from three to six times in pure solvent and the true detection limits in the presence of different matrix was achieved by optimisation of the plasma operating conditions. The lowest possible detection limits were obtained under different excitation conditions depending on the spectral characteristics of the selected prominent lines and the interfering matrix lines. There should be noted that the type of background as molecular bands must be taken into account in the optimization of the operating conditions in the determination of REE's in the presence of lutetium as matrix.

REFERENCES

1. P.W.J.M. Boumans, Basic concepts and characteristics of ICP-AES, in: Boumans (Ed.), Inductively Coupled Plasma Emission Spectroscopy, Part 1, Methodology, Instrumentation, and Performance, Wiley, New York, 1987, p. 100, Chapter 4.
2. J. Dennaud, A. Howes, E. Poussel, J.M. Mermet, *Spectrochim. Acta Part B* **56**, 101 (2001).
3. E. Abad-Peña, M.T. Larrea-Marin, M. Villanueva-Tagle, M. Simeón Pomares-Alfonso, *Spectroscopy Letters* **49**, 19 (2016).
4. S. Velichkov, E. Kostadinova, N. Daskalova, *Spectrochim. Acta Part B* **53** 1863 (1998).
5. N. Daskalova, S. Velichkov, P. Slavova, E. Ivanova, L. Aleksieva, *Spectrochim. Acta Part B* **52**, 257 (1997).
6. M. Stepan, P. Musil, E. Poussel, J.M. Mermet, *Spectrochim. Acta Part B* **56**, 443 (2001).
7. J.M. Mermet, *Anal. Chim. Acta* **250**, 85 (1991).
8. G.C.-Y. Chan, W.T. Chan, X. Mao, R.E. Russo, *Spectrochim. Acta Part B* **56**, 77 (2001).
9. C.Y. Chan, G.M. Hieftje, *Spectrochim. Acta Part B* **61**, 642 (2006).
10. M.W. Blades, G. Horlick, *Spectrochim. Acta Part B* **36**, 871 (1981).
11. H. Kawaguchi, T. Ito, A. Mizuike, *Spectrochim. Acta Part B* **36**, 615 (1981).
12. M. Murillo, J.M. Mermet, *Spectrochim. Acta Part B* **42**, 1151 (1987).
13. M. Carré, K. Lebas, M. Marichy, M. Mermet, E. Poussel, J.M. Mermet, *Spectrochim. Acta Part B* **50**, 271 (1995).
14. I. Novotny, I.C. Farinas, Wan-Jia-Iiang, E. Poussel, J.-M. Mermet, *Spectrochim. Acta Part B* **51**, 1517 (1996).
15. M. Grotti, E. Magi, R. Frache, *J. Anal. At. Spectrom.* **15**, 89 (2000).
16. P. Masson, A. Vives, D. Orignac, T. Prunet, *J. Anal. At. Spectrom.* **15**, 543 (2000).
17. J. Dennaud, A. Howes, E. Poussel, J.M. Mermet, *Spectrochim. Acta Part B* **56**, 101 (2001).
18. M. Iglésias, T. Vaculovic, J. Studynkova, E. Poussel, J.M. Mermet, *Spectrochim. Acta Part B* **59**, 1841 (2004).
19. A. Chazi, S. Qamar, *J. Chem. Sic. Pak.* **29**, 307 (2007).
20. A. Guimarães-Silva, J. de Lena, R. Froes, L. Costa, C. Nascentes, *J. Braz. Chem. Soc.* **23**, 753 (2012).
21. A. Oliveira, N. Baccan, S. Cadore, *J. Braz. Chem. Soc.* **23**, 838 (2012).
22. J.M. Mermet, Spectroscopic diagnostics: basic concepts, in: P.W.J.M. Boumans (Ed.), Inductively Coupled Plasma Emission Spectroscopy, Part 1, Methodology, Instrumentation and Performance, Wiley, New York, 1987, p. 353, Chapter 10.
23. A. Zaidel, V. Prokofev, S. Raiskii, V. Slavnyi, E. Ya Shreider, Tables of spectral lines, IFI / Plenum, New York, 1970.
24. J. Wysocka-Lisec, Spectrum Lines of Rare Earths Arranged by Wavelengths, Lubelskie Towarzyswo Naukowe, Lodz, 1970.
25. C. Dubuisson, E. Poussel, J. L. Todoli, Mermet, *Spectrochim. Acta B* **53**, 593 (1998).

ОПТИМИЗИРАНЕ НА РАБОТНИТЕ УСЛОВИЯ ПРИ ОПТИЧНАТА ЕМИСИОННА СПЕКТРОМЕТРИЯ С ИНДУКТИВНО СВЪРЗАНА ПЛАЗМА

Н. С. Величкова^{1*}, С. В. Величков², М. Г. Караджов¹, Н. Н. Даскалова²

¹ *Геологически институт, Българска Академия на Науките, ул. „Акад. Г. Бончев” бл. 24, 1113 София, България, e-mail: niaveli@geology.bas.bg*

² *Институт по обща и неорганична химия, Българска Академия на Науките, ул. „Акад. Г. Бончев” бл. 11, 1113 София, България, e-mail: nonidas@hotmail.com*

Постъпила на 8 ноември 2016 г.; приета на 22 декември 2016 г.

(Резюме)

Оптимизирането на работните условия беше изследвано с цел понижаване на границите на откриване при оптичната емисионна спектрометрия с 40.68 MHz индуктивно свързана плазма с радиално наблюдение (ИСП-ОЕС). Mg II 280.270 nm / Mg I 285.213 nm (Mg II / Mg I) интензитетно отношение беше използвано за оценка на твърдостта на работните условия в плазмата. Работните условия бяха променяни чрез вариране на входящата мощност, аерозол носещия и обгръщащия газови потоци. Получена е експерименталната зависимост между големината на Mg II / Mg I и температурата за възбуждане в ИСП. Резултатите показват, че условията за възбуждане в ИСП трябва да се променят от меки към твърди чрез вариране на входящата мощност и обгръщащия газов поток при оптималната стойност на аерозол-носещия поток. В този случай процесите на формирането и транспортирането на аерозолите остават едни същи при различните условия за възбуждане. Чрез промяна на работните условия в плазмата от меки до твърди бяха постигнати най-ниски граници на откриване при определяне на елементи в еднокомпонентни и многокомпонентни матрици, използвайки избраните аналитични линии с различни спектрални характеристики.

Ключови думи: *ИСП-ОЕС, Оптимизиране на работните условия, Следи от елементи, Граници на откриване*